

# Genome-wide CRISPR Screen Reveal Targets of Chiral Gold(I) Anticancer Compound in Mammalian Cells

Jong Hyun Kim, Samuel Ofori, Abderrahmane Tagmount, Chris D. Vulpe,\* and Samuel G. Awuah\*

Cite This: *ACS Omega* 2022, 7, 39197–39205

Read Online

ACCESS |



Metrics &amp; More

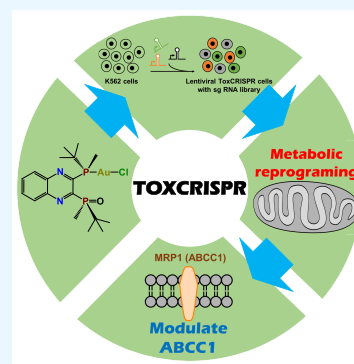


Article Recommendations



Supporting Information

**ABSTRACT:** Metal-based drugs, such as cisplatin and auranofin, are used for the treatment of cancer and rheumatoid arthritis, respectively. Auranofin and other gold-derived compounds have been shown to possess anticancer, anti-inflammatory, antimicrobial, and antiparasitic activity in preclinical and clinical trials. Unlike platinum agents which are known to target DNA, the target of gold is not well elucidated. To better understand the targets and effects of gold agents in mammalian cells, we used a targeted CRISPR (ToxCRISPR) screen in K562 cancer cells to identify genes that modulate cellular sensitivity to gold. We synthesized a novel chiral gold(I) compound, JHK-21, with potent anticancer activity. Among the most sensitizing hits were proteins involved in mitochondrial carriers, mitochondrial metabolism, and oxidative phosphorylation. Further analysis revealed that JHK-21 induced inner mitochondria membrane dysfunction and modulated ATP-binding cassette subfamily member C (ABCC1) function in a manner distinct from auranofin. Characterizing the therapeutic effects and toxicities of metallodrugs in mammalian cells is of growing interest to guide future drug discovery, and cellular and preclinical/clinical studies.



The development of efficacious transition-metal anticancer drugs is highly attractive yet a challenging goal in drug discovery. Platinum agents are first-line chemotherapy for several cancer types and are primordial to the development of improved metallodrugs.<sup>1–3</sup> However, toxic side effects and acquired tumor resistance to platinum therapy are major drawbacks.<sup>4–7</sup> Alternative efforts to develop other transition-metal-based anticancer agents such as Co,<sup>8</sup> Ti,<sup>9,10</sup> Ru,<sup>11</sup> Os,<sup>12,13</sup> and Au<sup>14–16</sup> have been stymied by unexplained cytotoxicity, rapid deactivation, poor pharmacokinetics, and poor *in vivo* potency.<sup>17</sup> Gold-based compounds have been applied as potent anticancer drug candidates in preclinical and clinical trials with great promise.<sup>18–26</sup> Recently, the FDA approved gold drug auranofin, used for the treatment of rheumatoid arthritis, was repurposed as an anticancer agent with promising outcomes.<sup>27</sup> Facile strategies to characterize the mechanism of action and targets of transition-metal compounds remain a challenge in metal-based drug discovery.

Chemical-genetic approaches involving high throughput yeast deletions and gene knockdown systems including RNA interference (RNAi) and short-hairpin RNA (shRNA) are powerful technologies to investigate drug-target interactions.<sup>28–33</sup> The recent discovery of CRISPR/Cas9 systems has provided robust and facile methods to edit mammalian genomes.<sup>34–36</sup> Pooled CRISPR screens have provided a powerful approach to identify drug targets, mechanisms of action, and resistance pathways of small-molecule drugs.<sup>37–39</sup> Herein we demonstrate a strategy using a toxicity targeted pooled CRISPR library to discover cellular targets and the

mechanism of action of JHK-21, a novel chiral gold(I)-phosphine compound.

The targeted CRISPR screen indicated that JHK-21 targets mitochondrial oxidative/bioenergetic processes, and biochemical studies demonstrated direct disruption of mitochondrial membrane potential. Additional factors modulating JHK-21 toxicity were identified including increased sensitivity in *ABCC1* (encoding the MRP1 drug/chemical exporter) mutants. Furthermore, we noted that loss of SPRED2, a negative regulator of the Ras-ERK pathway linked to the proteasome complex,<sup>24</sup> conferred resistance to JHK-21 treated cells. Our results highlight the utility of targeted CRISPR to comprehensively probe the activity of metallodrugs.

## RESULTS

**Synthesis and Characterization of JHK-21.** We explored the synthesis of chiral gold agents to discover novel gold compounds and structural scaffolds with high potency and distinct mechanisms.<sup>40–42</sup> The chiral compound JHK-21 was prepared as described in Figure 1A. Briefly, we reacted equimolar amounts of (*R,R*)-(-)-2,3-bis(*tert*-butylmethylphosphino)quinoxaline and phenanthroline gold-

Received: August 11, 2022

Accepted: October 6, 2022

Published: October 20, 2022



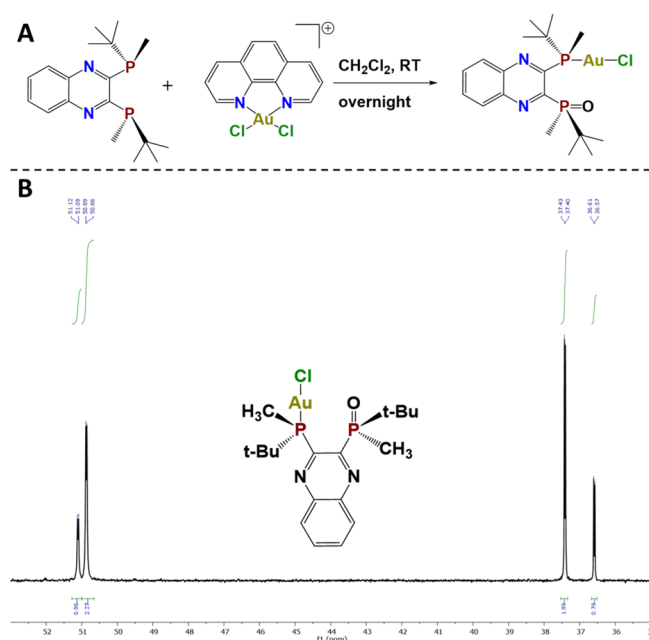


**Figure 1.** (A) Synthesis of the gold complex JHK-21 investigated in this study and (B)  $^{31}\text{P}\{^1\text{H}\}$  NMR spectrum of JHK-21.

(III) in dichloromethane at room temperature for 24 h (Figure 1A). The residue was purified by silica-gel flash column chromatography as a pale-yellow solid. JHK-21 was fully characterized by  $^1\text{H}$  NMR,  $^{31}\text{P}\{^1\text{H}\}$  NMR,  $^{13}\text{C}\{^1\text{H}\}$  NMR, high-resolution ESI mass spectrometry, and elemental analysis for purity (Supporting Information, Figures S1–S4). Both proton and carbon NMR spectroscopy revealed a complex without phenanthroline resonances. This observation is due to the strong  $\sigma$ -donating effect of the bisphosphine ligand, which rapidly displaces the phenanthroline ligand and reduces the Au(III) over a long reaction time. The oxidation of the phosphorus ligand under ambient conditions and chloride anions force the complex into a neutral Au(I) state. We highlight that the complex JHK-21 possesses a P-chirogenic ligand, which has the tendency to form diastereomers. What is observed in the NMR spectroscopy (both  $^1\text{H}$  and  $^{13}\text{C}$  NMR, ESI) is a classic diastereomeric ratio. All peaks agree with their

corresponding carbon atoms, and the integrated peaks also support the expected structure of JHK-21. The coupling arises from  $^{13}\text{C}$ – $^{31}\text{P}$ , and the neighboring small intensity peaks are from the other diastereomer, in a ratio of 1:2. The  $^{31}\text{P}\{^1\text{H}\}$  NMR spectrum is consistent with the proposed structure. The two P atoms have distinct chemical properties. P bonded to a gold atom is found at 37 ppm, and another P bonded to oxygen is found at 51 ppm. The two separate peaks are visible at each location due to the diastereomeric ratio, and each peak is a doublet due to typical P–P coupling (Figure 1B).

**Biological Activity of JHK-21.** We first investigated the biological activity of JHK-21 in human K562 cells. The compound inhibited K562 cells' growth with a 50% maximal inhibitory concentration ( $\text{IC}_{50}$ ) of 0.2  $\mu\text{M}$ , arrested cell cycle in the S phase by 24 h, and induced significant apoptosis within 48 h (Supporting Information).

**CRISPR-Cas9 Screen for Target Identification.** We used a targeted CRISPR-Cas9-based chemical genetics approach<sup>43–45</sup> to identify the mode of action of our metal-containing agent (Figure 2). We developed the ToxCRISPR KO library which targets 3675 genes involved in cellular toxicity response genes with 4–6 sgRNA in the LentiCRIPRV2 vector, an all-in-one vector containing both sgRNA and Cas9, as described in the Experimental Procedures and Supporting Information. To carry out the screen, we transduced  $50 \times 10^6$  K562 cells at 0.4 MOI, puromycin selected for 6 days, to develop a pooled mutant library. Three control and three exposure replicates of  $7.5 \times 10^6$  cells each (500 $\times$  representation) were used for screening. Exposed samples were treated with JHK-21 at the 48 h  $\text{IC}_{30}$  concentration (0.4  $\mu\text{M}$ ) to identify sensitive and resistant clones as compared to the untreated control (DMSO treated). At Day 7, the viability was approximately 60% of the control cells, and by the last day of the screen, the viability dropped to 30%. After 14 days, we isolated genomic DNA from untreated and JHK-21 treated cells and PCR-amplified sgRNA-encoding DNA constructs and quantitated sgRNA abundance by NGS. We identified mutants with significant differences in representation in the treated vs untreated samples as described in the Experimental Procedures. We applied three different analysis methods (MAGeCK, EdgeR, and DeSeq2) and compared the results across the approaches. For MAGeCK, we identified candidates at an FDR

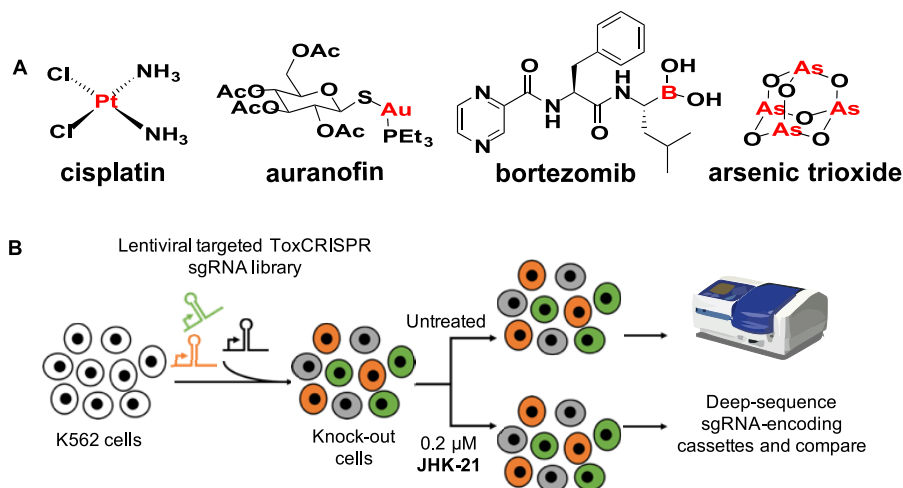


**Figure 2.** (A) Metal-/metalloid-based drugs used in the clinic. (B) Schematic of the pooled CRISPR-Cas9 screening approach to identify the cellular target and mechanism of action of JHK-21.

< 0.1 while for EdgeR and DeSeq2, which identify individual candidate sgRNA, we identified candidate genes for which two or more sgRNA had an FDR < 0.1. We compared the results across all three methods and further considered genes identified in two or more of these analysis approaches. Using these criteria, ten candidate genes increased resistance to JHK-21 when targeted and 14 genes increased sensitivity to JHK-21 when targeted. See the Supporting Information files for full results.

**Analysis of Genes That Sensitize K562 Cells to JHK-21.** Enrichment analysis using DAVID (<https://david.ncifcrf.gov/>) and Stringsdb (<https://string-db.org/>) of the 14 sensitive mutants from the CRISPR screen revealed enrichment of genes involved in mitochondrial function with nine (*ATP5I*, *NDUFS6*, *NFU1*, *AIFM1*, *GARS*, *SLC25A19*, *SLC25A46*, *SOD2*, *TIMM17A*) of 14 being mitochondrial (FDR <  $5.2 \times 10^{-6}$ , David) and six associated with inner mitochondrial membrane (*ATP5I*, *NDUFS6*, *AIRMI*, *SLC25A19*, *SOD2*, and *TIMM17A*). Genes involved in mitochondrial transport included *TIMM1*, *SLC25A19*, and *SLC25A46* and those involved in mitochondrial oxidative phosphorylation such as the oxidoreductases (*AIFM1*, *NDUFS6*, and *SOD2*) and the electron transport chain (*ATP5I* and *NFU1*). Full results are presented in the Supporting Information. These findings suggest that JHK-21 directly or indirectly alters mitochondrial metabolism or function.

We also identified gene knockouts that provided a protective effect and were enriched in the JHK-21 treated cell population. We did not identify significant enrichment of the ten candidates although four (*SUV39H*, *KDM6A*) were identified by Stringsdb as involved in histone modification and two are histone proteins (*HIST1H2BK*, *CENPA*).

**Validation of Individual Knockouts.** We carried out individual CRISPR targeting of candidate genes including *ABCC1*, which sensitized cells to JHK-21 when targeted, and *SPRED2*, which protected K562 cells to JHK-21. To investigate the cellular uptake of JHK-21 in wild-type and mutant K562 cells, we determined the cellular accumulation of JHK-21 in K562 cells by measuring gold content using inductively coupled optical emission spectroscopy (ICP-OES, Figure 3). We compared the uptake of gold to another gold compound, auranofin. K562 cells were treated with compounds at 5  $\mu$ M concentration for 12 h, and the cell pellets were subsequently digested and analyzed by ICP-OES. The

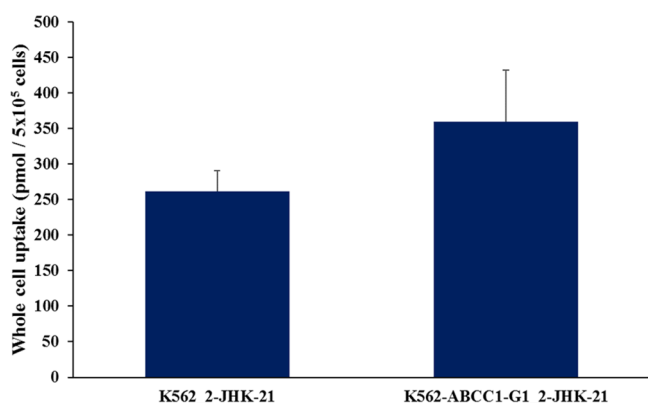


**Figure 3.** Cell uptake studies of JHK-21 in K562 and K562-ABCC1-G1. Cells were treated with 5  $\mu$ M of compound for 12 h ( $n = 3$ ).

uptake of JHK-21 was markedly lower than auranofin (Supporting Information). We found that three sgRNAs targeting *ABCC1* in K562 significantly enhanced susceptibility to JHK-21 in comparison to wild-type K562 as shown in Figure 4. Similarly, sgRNAs targeting *SPRED2* sgRNAs increased resistance to JHK-21 toxicity (Figure 4). These results confirm the findings of our pooled CRISPR screen.

**Cellular Response to JHK-21.** The ToxCRISPR screen implicated mitochondrial function in the biological effects of JHK-21, which led us to directly assess if JHK-21 targets mitochondrial function. We first assessed if JHK-21 disrupted mitochondrial oxidative respiration or induced changes to the mitochondria matrix. We assessed if JHK-21 interferes with mitochondrial respiration through real-time oxygen consumption rate measurement using a Seahorse XF96 analyzer. We measured the basal and maximal respiration of K562 and individual gene knockouts of K562. It was evident that wild-type K562 demonstrates higher maximal OCR than *ABCC1*, *ATP5I*, or *SPRED2* knockout cells. We then treated K562 cells with a 5  $\mu$ M concentration of JHK-21 by pneumatic injection. The compound induced significant inhibition of mitochondrial basal and maximal respiration (Figure 5). Taken together, our results suggest that JHK-21 alters cellular energy production via interaction with mitochondrial processes even at early time points.

Next, we examined the effect of JHK-21 on mitochondrial membrane potential (MMP) in K562 cells since MMP is a driver of ATP synthesis and helps maintain redox homeostasis. The mitochondrial membrane was significantly depolarized by JHK-21 based on the assessment of green fluorescent monomers of JC-1 in a similar manner to cyanide m-chlorophenyl hydrazone (CCCP). Interestingly, when K562 *ABCC1* KO cells were used, a higher population of cells with membrane depolarization was observed when compared to that of wild-type K562, consistent with increased intracellular levels of JHK-21 in the KO (Figure 6). These results demonstrate that JHK-21 alters the mitochondrial membrane potential.

## DISCUSSION

The ability to identify cellular targets of metallodrugs is crucial in understanding the mechanism of action as well as potential off-target effects within the host. Here we demonstrate for the first time the utility of a targeted CRISPR screening in a human cell line to determine the cellular modulators of sensitivity to a novel metal-based gold(I) compound, JHK-21. By focusing on a limited set of toxicity related genes, we were able to rapidly identify the functional mechanism underlying the observed cytotoxicity of JHK-21. While we cannot rule out that a genome-wide screen would not identify additional functional components involved in the cellular response to this compound, the focused approach on a limited subset of well annotated genes involved in cellular toxicity provided important insight into the functional effects of this compound. This strategy should be applicable to other metal-containing bioactive compounds, a class of biomedically relevant compounds whose mechanism of action has been elusive. We found that JHK-21 targets mitochondrial function by disrupting the mitochondrial membrane potential and inhibiting mitochondrial respiration in cells.

While the use of gold as therapeutics has been demonstrated in the clinic with the use of auranofin to treat rheumatoid arthritis, new bioactive gold-based agents have been hampered

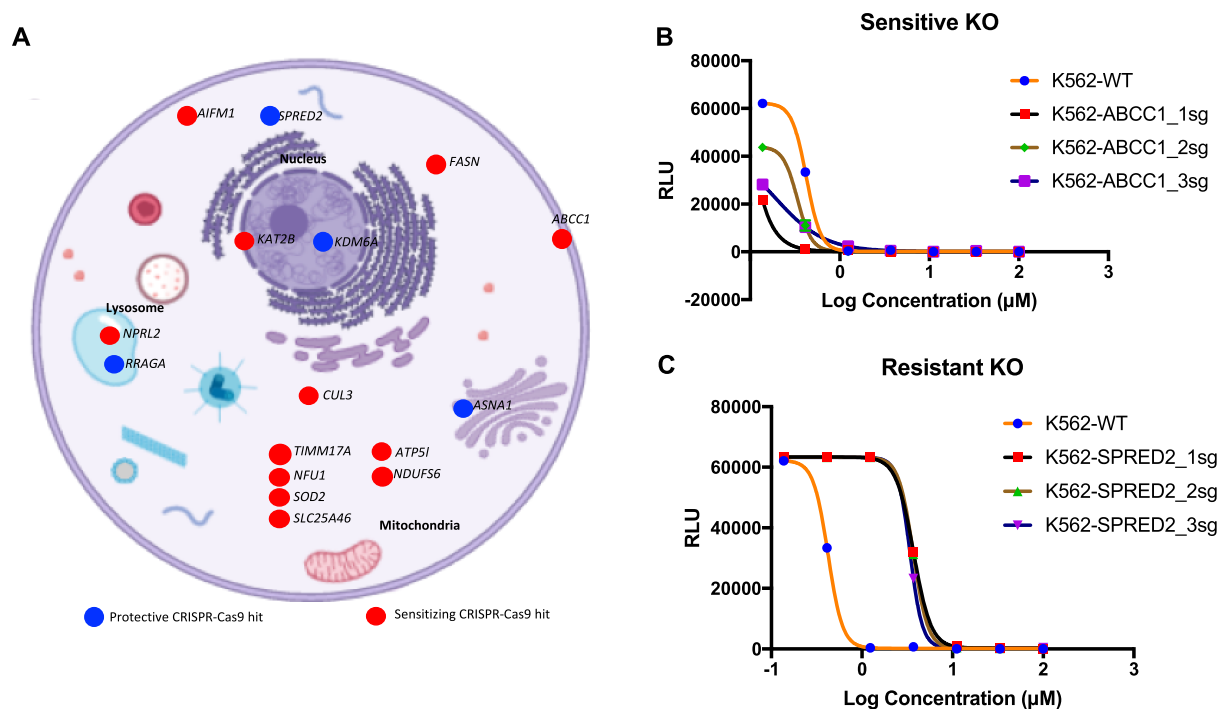


**Figure 4.** Results of the CRISPR screen for genes that sensitize cells to JHK-21. (A) Analysis of ToxCrisPR results. Candidate genes and their intracellular localization are illustrated with red dots, and the genes that confer protection to JHK-21 are shown in blue dots. (B, C) Validation of CRISPR using KO. Individual clones of ABCC1 KO and SPRED2 KO in K562 were generated using the same sgRNAs employed in the pooled ToxCrisPR screen. Cell viability using the CellTiter-Glo assay of K562-ABCC1 KO confirms sensitivity to JHK-21, and K562-SPRED2 confirms resistance to JHK-21.

by the lack of facile synthetic methods. The promising effects in repurposing auranofin to treat other disease indications including cancer and microbial infections in the clinic provide the impetus for gold drug discovery. We envisioned that expanding the chemical diversity of gold-based scaffolds would yield transformative biomedical outcomes. Thus, we utilized our nucleophile induced reductive elimination strategy to generate a tricoordinate gold(I), where a biologically tolerable chiral bisphosphine ligand was used. This new approach resulted in a novel tricoordinate gold(I) compound with potent cytotoxicity in cancer cells.

Despite effective clinical and preclinical treatment of cancer and rheumatoid arthritis by gold complexes, the molecular basis of gold drug action remains unclear. A number of targets have been suggested, including the following: (i) proteasome-associated deubiquitinases;<sup>24,46–48</sup> (ii) thiol-rich enzymes such as thioredoxin and glutathione reductase;<sup>49–52</sup> (iii) thiol-dependent proteases;<sup>53</sup> (iv) autophagy induction;<sup>54</sup> and superoxide/oxy radical ion generation.<sup>55</sup> Here, we demonstrate that JHK-21 targets mitochondrial processes to exploit cancer cell dependencies.

We focused on mitochondrial function as a potential JHK-21 target based on the ToxCrisPR screen. Our genetic approach clearly implicated mitochondrial oxidative phosphorylation, depicted in oxidoreductases (*AIFM1*, *NDUFS6*, and *SOD2*) and ETC genes (*ATP5I*, *NFU1*) as crucial modulators of K562 growth sensitivity to JHK-21. Although transition-metal complexes possess inherent redox properties, very few studies have been performed to characterize their impact on cellular mitochondrial respiration. We observed the inhibition of maximal respiration when K562 cells were treated with JHK-21. It is important to note that *AIFM1*, which appeared in our sensitizing hits, is a key regulator of mitochondria-mediated

apoptosis and is characterized as a NAD(P)H oxidoreductase. The deficiency of *AIFM1* in mice or humans is associated with decreased oxidative phosphorylation activity through mitochondria complex I and complex III activity. Inhibition of OXPHOS by JHK-21 is corroborated by the identification of NADH dehydrogenase (ubiquinone) iron-sulfur protein 6, which is a mitochondrial membrane complex I protein involved in the transfer of electrons from NADH to the respiratory chain. Additionally, the top sensitizing hit genes *ATP5I* and *NFU1* involved in the respiratory chain support the hypothesis that JHK-21 inhibits mitochondrial oxidative phosphorylation through complex I-mediated processes. Additionally, *FASN* is characterized as a metabolic oncogene implicated in tumor growth and survival. Targeting *FASN* represents an attractive therapeutic strategy. Additionally, a critical chaperone of neddylation known as glycyl tRNA synthetase (*GARS*), which is implicated in protein synthesis and lysine acetyltransferases (*KAT2B*) for post-transcriptional modification of histone, was identified as a sensitizing hit.

Metabolic reprogramming is a hallmark of a number of diseases, including cancer. The onset of cancer and its progression depends on mitochondrial metabolic function, which makes them vulnerable. Therefore, therapeutics that selectively modulate mitochondrial function could lead to targeted therapies.

The transport gene *TIMM17* is a carrier translocase of the inner mitochondrial membrane and appeared in the top sensitizing hits in response to JHK-21. Endogenous pre-sequence-containing precursors are delivered to the matrix and inner membrane in an inner membrane electrochemical potential ( $\Delta\psi$ )-dependent manner. The binding of molecules to *TIMM17* has the potential to potentiate the mitochondrial

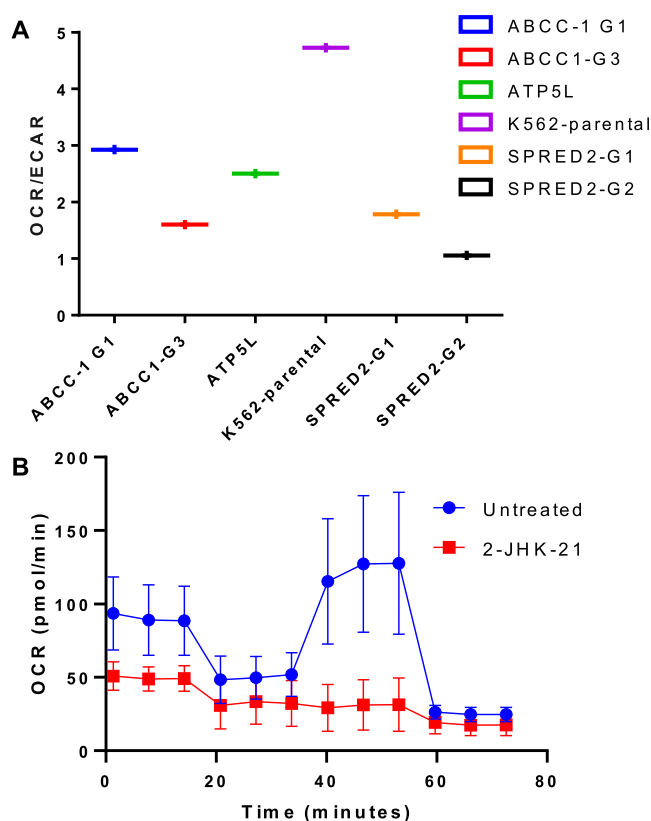


**Figure 5.** JHK-21 disrupts mitochondrial oxidative phosphorylation. (A) Real-time monitoring of the ratio of the oxygen consumption rate (OCR) and extracellular acidification rate (ECAR) of different isogenic K562 cells. (B) Inhibition of the OCR in K562 by JHK-21. Oligomycin (a complex V inhibitor), FCCP (a mitochondrial uncoupler), and rotenone/antimycin A (respiratory chain inhibitors) were added at intervals of 20 min. JHK-21 was added to K562 cells 12 h prior to bioenergetic measurements ( $n = 6$ ).

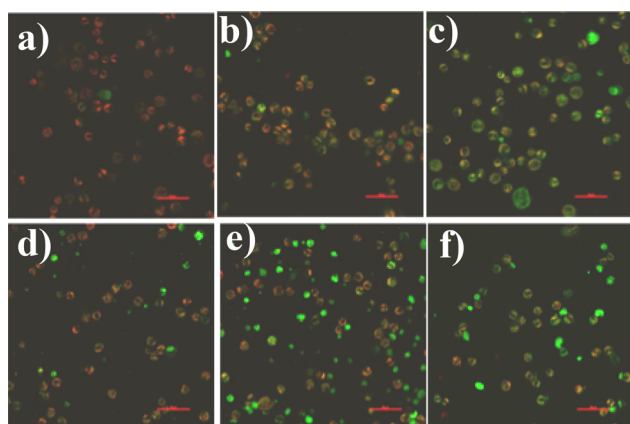


**Figure 6.** Images of K562 with JC-1 dye, overlay of green and red fluorescence (a–c). (a) Negative control (untreated), (b) 2-JHK-21 induced mitochondrial membrane potential ( $\Delta\psi_m$ ) loss, and (c) positive control, CCCP. (d) Negative control (ABCC1-G1 KO untreated), (e) 2-JHK-21 induced mitochondrial membrane potential ( $\Delta\psi_m$ ) loss, and (f) positive control, CCCP.

membrane potential, which is observed when K562 cells are treated with JHK-21.

Another transporter, which is an ATP-binding cassette transporter, ABCC1, is responsible for transporting a wide

range of molecules across cell membranes. Particularly, multi-drug resistance-associated protein (MRP) overexpression has been associated with chemotherapy resistance due to drug efflux in cancer cells.

Among the most protective sgRNAs were those against genes involved in histone modification (*HIST1H2BK* and *KDM6A*). Recent studies have identified molecular signatures of epigenetic regulation and chromatin architecture as pivotal modulators of mitochondrial function. Specifically, there appears to be a complex interplay between environmental factors, epigenetic signals, and mitochondrial metabolism. Since several components required for histone modification need intermediates of cellular metabolism including ATP, AcCoA, NADH, and  $\alpha$ -ketoglutarate for enzymatic function, it is important to delineate the mechanism that underlying response of gold therapy or resistance.

Mechanistic insights from our targeted CRISPR-Cas9 screen of the novel chiral gold(I) compound suggest that selective targeting of key mitochondria processes or metabolism represents an attractive and a clinically viable target to limit disease progression.

Finally, our CRISPR-Cas9 approach offers a functional platform to delineate mechanisms of bioactive transition-metal compounds. The molecular pathways by which metal-based agents such as JHK-21 modulate cellular sensitivity are not well understood. Together, our results highlight the power of knockout screening as a robust platform to interrogate biological pathways and enable drug target identification. This report represents the first systematic study to identify drug targets in mammalian cells of a novel gold antiproliferative agent, which possesses promising biological activity for therapeutic benefit.

## EXPERIMENTAL PROCEDURES

**Chemicals and Reagents.** 1,10-Phenanthroline was from Sigma-Aldrich and used without further purification or drying. Tetrachloroauric acid ( $\text{HAuCl}_4 \cdot 3\text{H}_2\text{O}$ ) was purchased from NANOPARTZ and used as received. ACS grade solvents were purchased from Pharmco-Aaper and used without further purification or drying. Deuterated solvents were purchased from Cambridge Isotope Laboratories and used as received. Silica gel for column chromatography (Silicycle, P/N: R10030B SiliaFlashF60, size: 40–63  $\mu\text{m}$ , Canada) was purchased from Silicycle. Aluminum backed silica-gel plates (20  $\times$  20  $\text{cm}^2$ ) were purchased from Silicycle (TLA-R10011B-323) and utilized for analytical thin-layer chromatography (TLC). The detailed synthetic procedures to obtain JHK-21 are in the [Supporting Information](#).

**Cell Lines and Cell Culture Conditions.** All K562 and knocked-out K562 cells were maintained in Roswell Park Memorial Institute (RPMI) 1640 medium. All cell lines were cultured in RPMI supplemented with 10% FBS, 1% penicillin/streptomycin, and 1% amphotericin. All cells were grown at 37  $^\circ\text{C}$  in a humidified atmosphere containing 5%  $\text{CO}_2$ .

**Pooled sgRNA Analyses. ToxCrispr KO Library.** The ToxCrispr Knockout library targets 3,675 protein-coding genes including the “S1500+” gene set prioritized by the NIEHS/NTP/Tox21 program along with genes in the environmental genome project ([https://egg.gs.washington.edu/finished\\_genes.html](https://egg.gs.washington.edu/finished_genes.html)) and a few other selected toxicant response related genes. The library contains 4 sgRNAs targeting each of the 3675 genes along with 500 nontargeting sgRNAs cloned into the LentiCRISPRv2 (Addgene #52961)

vector which was sequence verified for representation. Additional details on the development and validation of the ToxCRISPR library are presented in the [Supporting Information](#). The ToxCRISPR library was packaged in lentivirus and titer determined as described in the [Supporting Information](#).

**JHK-21 ToxCRISPR Screen.** 50 million K562 cells were transduced as in Sobh et al., 2019,<sup>56</sup> with the lentiviral packaged ToxCrispr Library at a MOI of 0.4. 48 h post-transduction, the cells were selected against 2  $\mu\text{g}/\text{mL}$  puromycin for 6 days. Three aliquots of 20 million cells were frozen and stored to serve as a reference for the representation at Day 1 (i.e., first day of screen). CRISPR screens were performed in T75 flasks, with 7.5 million per replicate to achieve a 500 $\times$  coverage, in 30 mL RPMI 1640 supplemented with 10% FBS and 1 $\times$  pen/strep. The conditions were the following: untreated cells (control) and 0.4  $\mu\text{M}$  JHK-21 for 14 days (i.e., 14 doublings of untreated WT K562). Each condition was performed in triplicate. The medium was replaced every 48 h by spinning down the cells at 300g for 5 min, and 7.5 million cells were reseeded at each medium change to maintain 500 $\times$  coverage. Genomic DNA from 7.5 million cells for each replicate was extracted using the DNeasy Blood & Tissue Kit (Qiagen) following the manufacturer's instructions. Amplicons for NGS illumina sequencing were generated using the two-step PCR described in detail in Sobh et al., 2019.<sup>56</sup>

In brief, for each sample, the gRNA region was first PCR amplified using the high fidelity Herculase II Fusion DNA Polymerase kit (Agilent) and the pair of primers CRISPR1-FOR and CRISPR1-REV (PCR1). The amplicon libraries for NGS were prepared and barcoded by carrying out a second PCR (PCR2) using a combination of a common forward primer (CRISPR2-FOR) and a sample specific reverse primer (CRISPR2-REV#) incorporating respectively the P5 and the P7+barcode adapters. For each sample, four 100  $\mu\text{L}$  PCR1 reactions were performed using 10  $\mu\text{g}$  genomic DNA template per reaction and 18 cycles. The PCR1 products were pooled for each sample followed by two 100  $\mu\text{L}$  PCR2 reactions. PCR2 was carried out using 5  $\mu\text{L}$  PCR1 product per reaction and 20 cycles producing 358 bp amplicon libraries.

The sequence of the primers used to prepare the amplicon libraries as well as the barcodes are listed in the [Supporting Information](#). The amplicons were gel purified using the QIAquick Gel Extraction Kit (Qiagen) and quantified using the Qubit HS dsDNA assay (ThermoFisher). Equimolar amounts (875 ng) of each amplicon library were multiplexed in one pool. The library size and concentration were confirmed by TapeStation (Agilent). The sequencing was performed at the Interdisciplinary Center for Biotechnology Research (ICBR), University of Florida at Gainesville, using the NextSeq500 high throughput single read 75 cycles platform (Illumina).

**CRISPR-seq Data Analysis Results for the NS-910 Project.** FASTQC tools (version 0.11.8)<sup>57</sup> were applied to compressed fastq-files received from the sequencing facility to check read quality. Bowtie (version 1.2.2) was used to align ToxCRISPR sgRNAs against reads per each condition to generate the raw count table using Samtools<sup>58</sup> and a R wrapper.<sup>59</sup> The raw count table was used as input for MAGeCK, edgeR,<sup>60,61</sup> and DESeq2<sup>62</sup> packages (with default parameters for normalization). Consolidated and annotated summary tables with

sgRNA differential representation were generated for each comparison with adjusted p-values.<sup>63</sup>

**Individual sgRNA Validation. Method: sgRNA Cloning, Lentivirus Production, and Transduction.** The guide RNAs (gRNAs) targeting the *ABCC1*, *SPRED2*, and *ATPSL* genes were selected from the Brunello genome-wide CRISPR pooled gRNAs library<sup>64</sup>

The gRNAs had the following sequences:

ABCC1 (gRNA-1) (AAAATGTGATTGGCCCCAAG),  
ABCC1 (gRNA-2) (AACCTGACAGCATCGAGCGA),  
ABCC1 (gRNA-3) (AGTACACGGAAAGCTTGACC),  
SPRED2 (gRNA-1) (AGTCTGAGGAGTCCACGTAG),  
SPRED2 (gRNA-2) (TCCAACGTTTCATCACTGGA),  
SPRED2 (gRNA-3) (CTGTGGGGTATGAGTCGTGG),  
ATPSL (gRNA-1) (CTCACCGTTCACCAGCGCCG),  
and ATPSL (gRNA-3) (ATAGTCAATAGTGCTCAGAC).

Each gRNA was cloned in the lentiviral vector LentiCRISPRv2 (Plasmid #52961, Addgene) using the golden gate assembly strategy described in detail.<sup>65</sup>

To produce lentiviruses, LentiCRISPRv2 constructs harboring each of the *ABCC1*, *SPRED2*, or *ATPSL* gRNAs were cotransfected in HEK293T cells with the envelope PMD2.G and packaging psPAX2 plasmids. In brief, HEK293T cells were seeded in T25-cm2 tissue culture flasks the day preceding the cotransfection. One hour before the transfection, the medium was replaced with 2.25 mL Optimem medium (ThermoFisher).

For each of the gRNAs, the DNA mixtures consisted of 3.4  $\mu\text{g}$  lentiCRISPRv2-gene target plasmid, 1.7  $\mu\text{g}$  PMD2.G, and 2.6  $\mu\text{g}$  psPAX2 diluted in 700  $\mu\text{L}$  Optimem and 35  $\mu\text{L}$  plus reagent (ThermoFisher), and the lipofectamine mix consisted of 700  $\mu\text{L}$  Optimem and 17.25  $\mu\text{L}$  lipofectamine 2000 (ThermoFisher). The two mixtures were incubated for 5 min at room temperature and then combined and incubated at room temperature for 20 min. The lipofectamine-DNA complex was added to the HEK293T cells, and the cells were then incubated for 6 h at 37  $^{\circ}\text{C}$  and 5%  $\text{CO}_2$ . The transfection medium was replaced with 6 mL of lentivirus harvest medium (DMEM high glucose, 10% FBS, 1 $\times$  penicillin/streptomycin, 1% BSA). The lentiviruses were harvested 48 h post-transfection as follows: cell culture medium was collected and centrifuged at 3000 rpm for 10 min at 4  $^{\circ}\text{C}$ . The supernatant was syringe filtered through a 0.45  $\mu\text{m}$  PES sterile filter (Sartorius). To concentrate the lentiviruses, 2 mL (1/4 of the supernatant volume) of Lenti-X concentrator (Takara Bio) was mixed with the filtrate. The mixture was incubated on ice for 2 h 30 min and then centrifuged at 1500g for 45 min at 4  $^{\circ}\text{C}$ . The obtained pellet was resuspended in 300  $\mu\text{L}$  of harvest media and stored at  $-80^{\circ}\text{C}$ .

K562 cells were transduced separately with each of the *ABCC1*, *SPRED2*, and *ATPSL* lentiviral preparations using the spinoculation method. In brief, 2.5 million K562 cells were seeded in a 12-well plate in 2 mL of RPMI 1640 medium supplemented with 10% FBS and 1 $\times$  penicillin/streptomycin. Polybrene (8  $\mu\text{g}/\text{mL}$  final concentration) and 10  $\mu\text{L}$  of the lentiviral solution were added to the cells and mixed gently up and down. The 12-well plate was centrifuged at 1000g for 90 min at 34  $^{\circ}\text{C}$ . After centrifugation, the cells were transferred to 15 mL conical tubes and pelleted (300g for 5 min). The cell pellet was resuspended in 6 mL of RPMI 1640 supplemented with 10% FBS and 1 $\times$  antibiotic penicillin/streptomycin and cultivated in a T25-cm2 tissue culture flask for 48 h. The transduced cells that integrated the lentiviral genome were

then selected in medium supplemented with 2  $\mu\text{g}/\text{mL}$  puromycin for 6 days.

**Mitochondrial Membrane Potential (JC-1 Assay).** K562 cells were plated at a density of  $5 \times 10^5$  cells/plate using a glass bottom Petri dish fitted with a #1.5 coverslip with a final volume of 1.5 mL. JHK-21 was prepared as a stock in DMSO/RPMI (2:8) and added at a final concentration of 10  $\mu\text{M}$ . The cells were treated for 6 h at this concentration. CCCP was prepared as a stock in DMSO and added at a final concentration of 100  $\mu\text{M}$ , and the cells were treated for 1 h. This was used as a positive control. After the indicated treatment time, a working solution of the JC-1 dye (Cayman Chemicals) was prepared by adding 100  $\mu\text{L}$  of dye into 900  $\mu\text{L}$  of RPMI. Note: the working solution of JC-1 should always be prepared fresh and not stored for long-term use. Then, 100  $\mu\text{L}/\text{mL}$  of RPMI was added to the cells and incubated at 37  $^\circ\text{C}$  for 20 min. Prior to imaging, the media was removed and replaced with room temperature PBS (2 mL). The cells were then visualized using confocal microscopy on a Nikon A1R inverted confocal microscope. J-aggregates were imaged with excitation/emission = 510/590 nm and J-monomers with excitation/emission = 488/525 nm. Each image is representative of three technical replicates.

## ■ ASSOCIATED CONTENT

### SI Supporting Information

The Supporting Information is available free of charge at <https://pubs.acs.org/doi/10.1021/acsomega.2c05166>.

All synthetic procedures, chemical experiments, biological experiments, and characterization data (PDF)

ToxCRISPR library, raw counts, analysis, primers used to prepare the amplicon libraries as well as the barcodes (XLSX)

## ■ AUTHOR INFORMATION

### Corresponding Authors

**Chris D. Vulpe** – Department of Physiological Sciences, College of Veterinary Medicine, University of Florida, Gainesville, Florida 32611, United States; [orcid.org/0000-0001-5134-8929](https://orcid.org/0000-0001-5134-8929); Email: [cvulpe@ufl.edu](mailto:cvulpe@ufl.edu)

**Samuel G. Awuah** – Department of Chemistry, University of Kentucky, Lexington, Kentucky 40506, United States; Department of Pharmaceutical Sciences, College of Pharmacy and Markey Cancer Center, University of Kentucky, Lexington, Kentucky 40536, United States; [orcid.org/0000-0003-4947-7283](https://orcid.org/0000-0003-4947-7283); Email: [awuah@uky.edu](mailto:awuah@uky.edu)

### Authors

**Jong Hyun Kim** – Department of Chemistry, University of Kentucky, Lexington, Kentucky 40506, United States

**Samuel Ofori** – Department of Chemistry, University of Kentucky, Lexington, Kentucky 40506, United States

**Abderrahmane Tagmout** – Department of Physiological Sciences, College of Veterinary Medicine, University of Florida, Gainesville, Florida 32611, United States

Complete contact information is available at:

<https://pubs.acs.org/doi/10.1021/acsomega.2c05166>

### Funding

We are grateful to the University of Kentucky for funding. This work was funded by National Institutes of Health/NCI grant R01CA258421-01 (S.G.A.).

## Notes

The authors declare no competing financial interest.

## ■ ACKNOWLEDGMENTS

We would like to acknowledge all of those who helped contribute to the project. We would like to thank all of the facilities at the University of Kentucky, who provided support in completion of the experiments detailed in this manuscript. The UK NMR Center is supported by the NSF (CHE-997738), and the UK X-ray facility is supported by the MRI program from NSF (CHE-1625732). For the flow cytometry experiments we would like to thank Greg Bauman Ph.D. UK Flow Cytometry and Immune Function Core is supported by the Office of the Vice President of Research, the Markey Cancer Center, and NCI Center Core Support Grant (P30 CA177558). For microscopy, we would like to thank Thomas Wilkop Ph.D. We would also like to thank Tomoko Sengoku Ph.D. and Mr. Michael Alstott for the support with our redox metabolism experiments, supported by the shared resource(s) of the University of Kentucky Markey Cancer Center (P30CA177558).

## ■ REFERENCES

- (1) Lefebvre, J.; Glezerman, I. G. Anticancer Drugs and the Kidney. In *Critical Care Nephrology*, 3rd ed.; Ronco, C., Bellomo, R., Kellum, J. A., Ricci, Z., Eds.; Elsevier: Philadelphia, 2019; Chapter 217, pp 1302–1305.e2.
- (2) Piccart, M. J.; Lamb, H.; Vermorken, J. B. Current and future potential roles of the platinum drugs in the treatment of ovarian cancer. *Annals of Oncology* **2001**, *12* (9), 1195–1203.
- (3) Goffin, J.; Lacchetti, C.; Ellis, P. M.; Ung, Y. C.; Evans, W. K. First-Line Systemic Chemotherapy in the Treatment of Advanced Non-small Cell Lung Cancer: A Systematic Review. *Journal of Thoracic Oncology* **2010**, *5* (2), 260–274.
- (4) Johnstone, T. C.; Park, G. Y.; Lippard, S. J. Understanding and improving platinum anticancer drugs—phenanthriplatin. *Anticancer Res.* **2014**, *34* (1), 471–476.
- (5) Brabec, V.; Kasparkova, J. Modifications of DNA by platinum complexes: Relation to resistance of tumors to platinum antitumor drugs. *Drug Resistance Updates* **2005**, *8* (3), 131–146.
- (6) Chabner, B. A.; Roberts, T. G. Chemotherapy and the war on cancer. *Nature Reviews Cancer* **2005**, *5* (1), 65–72.
- (7) Kelland, L. The resurgence of platinum-based cancer chemotherapy. *Nature Reviews Cancer* **2007**, *7* (8), 573–584.
- (8) Slator, C.; Molphy, Z.; McKee, V.; Long, C.; Brown, T.; Kellett, A. Di-copper metallodrugs promote NCI-60 chemotherapy via singlet oxygen and superoxide production with tandem TA/TA and AT/AT oligonucleotide discrimination. *Nucleic Acids Res.* **2018**, *46* (6), 2733–2750.
- (9) Fernández-Gallardo, J.; Elie, B. T.; Sadhukha, T.; Prabha, S.; Sanaú, M.; Rotenberg, S. A.; Ramos, J. W.; Contel, M. Heterometallic titanium–gold complexes inhibit renal cancer cells in vitro and in vivo. *Chemical Science* **2015**, *6* (9), 5269–5283.
- (10) Mui, Y. F.; Fernández-Gallardo, J.; Elie, B. T.; Gubran, A.; Maluenda, I.; Sanaú, M.; Navarro, O.; Contel, M. Titanocene-Gold Complexes Containing N-Heterocyclic Carbene Ligands Inhibit Growth of Prostate, Renal, and Colon Cancers in Vitro. *Organometallics* **2016**, *35* (9), 1218–1227.
- (11) Zeng, L.; Gupta, P.; Chen, Y.; Wang, E.; Ji, L.; Chao, H.; Chen, Z.-S. The development of anticancer ruthenium(II) complexes: from single molecule compounds to nanomaterials. *Chem. Soc. Rev.* **2017**, *46* (19), 5771–5804.
- (12) Hearn, J. M.; Romero-Canelón, I.; Munro, A. F.; Fu, Y.; Pizarro, A. M.; Garnett, M. J.; McDermott, U.; Carragher, N. O.; Sadler, P. J. Potent organo-osmium compound shifts metabolism in epithelial ovarian cancer cells. *Proc. Natl. Acad. Sci. U. S. A.* **2015**, *112* (29), E3800–E3805.

- (13) van Rijt, S. H.; Peacock, A. F. A.; Johnstone, R. D. L.; Parsons, S.; Sadler, P. J. Organometallic Osmium(II) Arene Anticancer Complexes Containing Picolinate Derivatives. *Inorg. Chem.* **2009**, *48* (4), 1753–1762.
- (14) Berners-Price, S. J.; Filipovska, A. Gold compounds as therapeutic agents for human diseases. *Metalomics* **2011**, *3* (9), 863–873.
- (15) Bertrand, B.; Casini, A. A golden future in medicinal inorganic chemistry: the promise of anticancer gold organometallic compounds. *Dalton Transactions* **2014**, *43* (11), 4209–4219.
- (16) Tong, K.-C.; Lok, C.-N.; Wan, P.-K.; Hu, D.; Fung, Y. M. E.; Chang, X.-Y.; Huang, S.; Jiang, H.; Che, C.-M. An anticancer gold(III)-activated porphyrin scaffold that covalently modifies protein cysteine thiols. *Proc. Natl. Acad. Sci. U. S. A.* **2020**, *117* (3), 1321–1329.
- (17) Mjos, K. D.; Orvig, C. Metallo drugs in Medicinal Inorganic Chemistry. *Chem. Rev.* **2014**, *114* (8), 4540–4563.
- (18) Altaf, M.; Casagrande, N.; Mariotto, E.; Baig, N.; Kawde, A.-N.; Corona, G.; Larcher, R.; Borghese, C.; Pavan, C.; Seliman, A. A.; Aldinucci, D.; Isab, A. A. Potent In Vitro and In Vivo Anticancer Activity of New Bipyridine and Bipyrimidine Gold (III) Dithiocarbamate Derivatives. *Cancers (Basel)* **2019**, *11* (4), 474.
- (19) Barnard, P. J.; Berners-Price, S. J. Targeting the mitochondrial cell death pathway with gold compounds. *Coord. Chem. Rev.* **2007**, *251* (13), 1889–1902.
- (20) Marcon, G.; Carotti, S.; Coronello, M.; Messori, L.; Mini, E.; Orioli, P.; Mazzei, T.; Cinellu, M. A.; Minghetti, G. Gold(III) Complexes with Bipyridyl Ligands: Solution Chemistry, Cytotoxicity, and DNA Binding Properties. *J. Med. Chem.* **2002**, *45* (8), 1672–1677.
- (21) Marzano, C.; Ronconi, L.; Chiara, F.; Giron, M. C.; Faustini, I.; Cristofori, P.; Trevisan, A.; Fregona, D. Gold(III)-dithiocarbamate anticancer agents: activity, toxicology and histopathological studies in rodents. *Int. J. Cancer* **2011**, *129* (2), 487–96.
- (22) Messori, L.; Abbate, F.; Marcon, G.; Orioli, P.; Fontani, M.; Mini, E.; Mazzei, T.; Carotti, S.; O'Connell, T.; Zanello, P. Gold(III) Complexes as Potential Antitumor Agents: Solution Chemistry and Cytotoxic Properties of Some Selected Gold(III) Compounds. *J. Med. Chem.* **2000**, *43* (19), 3541–3548.
- (23) Messori, L.; Marcon, G.; Orioli, P. Gold(III) Compounds as New Family of Anticancer Drugs. *Bioinorganic Chemistry and Applications* **2003**, *1* (2), 177–187.
- (24) Milacic, V.; Dou, Q. P. The tumor proteasome as a novel target for gold(III) complexes: implications for breast cancer therapy. *Coordination chemistry reviews* **2009**, *253* (11–12), 1649–1660.
- (25) To, Y. F.; Sun, R. W.-Y.; Chen, Y.; Chan, V. S.-F.; Yu, W.-Y.; Tam, P. K.-H.; Che, C.-M.; Lin, C.-L. S. Gold(III) porphyrin complex is more potent than cisplatin in inhibiting growth of nasopharyngeal carcinoma in vitro and in vivo. *Int. J. Cancer* **2009**, *124* (8), 1971–1979.
- (26) National Library of Medicine. Auranofin in Decreasing Pain in Patients With Paclitaxel-Induced Pain Syndrome. 2014 Feb - 2016 Nov. Identifier NCT02063698. [ClinicalTrials.gov](https://clinicaltrials.gov) (US)
- (27) National Library of Medicine. A Phase I Phase II Two-Step Study of the Oral Gold Compound Auranofin in Chronic Lymphocytic Leukemia (CLL)/ Small Lymphocytic Lymphoma (SLL)/ Prolymphocytic Lymphoma (PLL). 2011 Sept - 2016 Sept. Identifier NCT01419691. [ClinicalTrials.gov](https://clinicaltrials.gov) (US)
- (28) Bassik, M. C.; Kampmann, M.; Lebbink, R. J.; Wang, S.; Hein, M. Y.; Poser, I.; Weibezahn, J.; Horlbeck, M. A.; Chen, S.; Mann, M.; Hyman, A. A.; Leproust, E. M.; McManus, M. T.; Weissman, J. S. A systematic mammalian genetic interaction map reveals pathways underlying ricin susceptibility. *Cell* **2013**, *152* (4), 909–22.
- (29) Kampmann, M.; Bassik, M. C.; Weissman, J. S. Integrated platform for genome-wide screening and construction of high-density genetic interaction maps in mammalian cells. *Proc. Natl. Acad. Sci. U. S. A.* **2013**, *110* (25), E2317–26.
- (30) Gregori-Puigjané, E.; Setola, V.; Hert, J.; Crews, B. A.; Irwin, J. J.; Loukine, E.; Marnett, L.; Roth, B. L.; Shoichet, B. K. Identifying mechanism-of-action targets for drugs and probes. *Proc. Natl. Acad. Sci. U.S.A.* **2012**, *109* (28), 11178–11183.
- (31) Lamb, J.; Crawford, E. D.; Peck, D.; Modell, J. W.; Blat, I. C.; Wrobel, M. J.; Lerner, J.; Brunet, J.-P.; Subramanian, A.; Ross, K. N.; Reich, M.; Hieronymus, H.; Wei, G.; Armstrong, S. A.; Haggarty, S. J.; Clemons, P. A.; Wei, R.; Carr, S. A.; Lander, E. S.; Golub, T. R. The Connectivity Map: Using Gene-Expression Signatures to Connect Small Molecules, Genes, and Disease. *Science* **2006**, *313* (5795), 1929–1935.
- (32) Parsons, A. B.; Lopez, A.; Givoni, I. E.; Williams, D. E.; Gray, C. A.; Porter, J.; Chua, G.; Sopko, R.; Brost, R. L.; Ho, C.-H.; Wang, J.; Ketela, T.; Brenner, C.; Brill, J. A.; Fernandez, G. E.; Lorenz, T. C.; Payne, G. S.; Ishihara, S.; Ohya, Y.; Andrews, B.; Hughes, T. R.; Frey, B. J.; Graham, T. R.; Andersen, R. J.; Boone, C. Exploring the Mode-of-Action of Bioactive Compounds by Chemical-Genetic Profiling in Yeast. *Cell* **2006**, *126* (3), 611–625.
- (33) Schenone, M.; Dancik, V.; Wagner, B. K.; Clemons, P. A. Target identification and mechanism of action in chemical biology and drug discovery. *Nat. Chem. Biol.* **2013**, *9* (4), 232–40.
- (34) Ran, F. A.; Hsu, P. D.; Wright, J.; Agarwala, V.; Scott, D. A.; Zhang, F. Genome engineering using the CRISPR-Cas9 system. *Nat. Protoc.* **2013**, *8* (11), 2281–2308.
- (35) Mali, P.; Yang, L.; Esvelt, K. M.; Aach, J.; Guell, M.; DiCarlo, J. E.; Norville, J. E.; Church, G. M. RNA-Guided Human Genome Engineering via Cas9. *Science* **2013**, *339* (6121), 823–826.
- (36) Cong, L.; Ran, F. A.; Cox, D.; Lin, S.; Barretto, R.; Habib, N.; Hsu, P. D.; Wu, X.; Jiang, W.; Marraffini, L. A.; Zhang, F. Multiplex Genome Engineering Using CRISPR/Cas Systems. *Science* **2013**, *339* (6121), 819–823.
- (37) Wang, T.; Wei, J. J.; Sabatini, D. M.; Lander, E. S. Genetic Screens in Human Cells Using the CRISPR-Cas9 System. *Science* **2014**, *343* (6166), 80–84.
- (38) Deans, R. M.; Morgens, D. W.; Okesli, A.; Pillay, S.; Horlbeck, M. A.; Kampmann, M.; Gilbert, L. A.; Li, A.; Mateo, R.; Smith, M.; Glenn, J. S.; Carette, J. E.; Khosla, C.; Bassik, M. C. Parallel shRNA and CRISPR-Cas9 screens enable antiviral drug target identification. *Nat. Chem. Biol.* **2016**, *12* (5), 361–6.
- (39) Gupta, A.; Okesli-Armlovich, A.; Morgens, D.; Bassik, M. C.; Khosla, C. A genome-wide analysis of targets of macrolide antibiotics in mammalian cells. *J. Biol. Chem.* **2020**, *295* (7), 2057–2067.
- (40) Dennis, E. K.; Kim, J. H.; Parkin, S.; Awuah, S. G.; Garneau-Tsodikova, S. Distorted Gold(I)-Phosphine Complexes as Antifungal Agents. *J. Med. Chem.* **2020**, *63* (5), 2455–2469.
- (41) Kim, J. H.; Reeder, E.; Parkin, S.; Awuah, S. G. Gold(I/III)-Phosphine Complexes as Potent Antiproliferative Agents. *Sci. Rep.* **2019**, *9* (1), 12335.
- (42) Gukathasan, S.; Parkin, S.; Awuah, S. G. Cyclometalated Gold(III) Complexes Bearing DACH Ligands. *Inorg. Chem.* **2019**, *58* (14), 9326–9340.
- (43) Gilbert, L. A.; Larson, M. H.; Morsut, L.; Liu, Z.; Brar, G. A.; Torres, S. E.; Stern-Ginossar, N.; Brandman, O.; Whitehead, E. H.; Doudna, J. A.; Lim, W. A.; Weissman, J. S.; Qi, L. S. CRISPR-mediated modular RNA-guided regulation of transcription in eukaryotes. *Cell* **2013**, *154* (2), 442–51.
- (44) Perez-Pinera, P.; Kocak, D. D.; Vockley, C. M.; Adler, A. F.; Kabadi, A. M.; Polstein, L. R.; Thakore, P. I.; Glass, K. A.; Ousterout, D. G.; Leong, K. W.; Guilak, F.; Crawford, G. E.; Reddy, T. E.; Gersbach, C. A. RNA-guided gene activation by CRISPR-Cas9-based transcription factors. *Nat. Methods* **2013**, *10* (10), 973–6.
- (45) Shalem, O.; Sanjana, N. E.; Zhang, F. High-throughput functional genomics using CRISPR-Cas9. *Nature reviews. Genetics* **2015**, *16* (5), 299–311.
- (46) Huang, H.; Liao, Y.; Liu, N.; Hua, X.; Cai, J.; Yang, C.; Long, H.; Zhao, C.; Chen, X.; Lan, X.; Zang, D.; Wu, J.; Li, X.; Shi, X.; Wang, X.; Liu, J. Two clinical drugs deubiquitinase inhibitor auranofin and aldehyde dehydrogenase inhibitor disulfiram trigger synergistic anti-tumor effects in vitro and in vivo. *Oncotarget* **2016**, *7* (3), 2796–808.

- (47) Zou, T.; Zhang, J.-J.; Cao, B.; Tong, K.-C.; Lok, C.-N.; Che, C.-M. Deubiquitinases as Anticancer Targets of Gold Complexes. *Isr. J. Chem.* **2016**, *56* (9–10), 825–833.
- (48) Zhang, J.-J.; Ng, K.-M.; Lok, C.-N.; Sun, R. W.-Y.; Che, C.-M. Deubiquitinases as potential anti-cancer targets for gold(III) complexes. *Chem. Commun.* **2013**, *49* (45), 5153–5155.
- (49) Schuh, E.; Pflüger, C.; Citta, A.; Folda, A.; Rigobello, M. P.; Bindoli, A.; Casini, A.; Mohr, F. Gold(I) Carbene Complexes Causing Thioredoxin 1 and Thioredoxin 2 Oxidation as Potential Anticancer Agents. *J. Med. Chem.* **2012**, *55* (11), 5518–5528.
- (50) Bindoli, A.; Rigobello, M. P.; Scutari, G.; Gabbiani, C.; Casini, A.; Messori, L. Thioredoxin reductase: A target for gold compounds acting as potential anticancer drugs. *Coordination Chemistry Reviews* **2009**, *253*, 1692–1707.
- (51) Deponte, M.; Urig, S.; Arscott, L. D.; Fritz-Wolf, K.; Reau, R.; Herold-Mende, C.; Koncarevic, S.; Meyer, M.; Davioud-Charvet, E.; Ballou, D. P.; Williams, C. H., Jr.; Becker, K. Mechanistic studies on a novel, highly potent gold-phosphole inhibitor of human glutathione reductase. *J. Biol. Chem.* **2005**, *280* (21), 20628–37.
- (52) Urig, S.; Fritz-Wolf, K.; Reau, R.; Herold-Mende, C.; Toth, K.; Davioud-Charvet, E.; Becker, K. Undressing of phosphine gold(I) complexes as irreversible inhibitors of human disulfide reductases. *Angew. Chem., Int. Ed. Engl.* **2006**, *45* (12), 1881–6.
- (53) Rohozková, D.; Steven, F. S. Gold-containing drugs and the control of proteolytic enzymes. *Br. J. Pharmacol.* **1983**, *79* (1), 181–189.
- (54) Tian, S.; Siu, F.-M.; Kui, S. C. F.; Lok, C.-N.; Che, C.-M. Anticancer gold(I)-phosphine complexes as potent autophagy-inducing agents. *Chem. Commun.* **2011**, *47* (33), 9318–9320.
- (55) Roisman, F. R.; Walz, D. T.; Finkelstein, A. E. Superoxide radical production by human leukocytes exposed to immune complexes: inhibitory action of gold compounds. *Inflammation* **1983**, *7* (4), 355–62.
- (56) Sobh, A.; Loguinov, A.; Yazici, G. N.; Zeidan, R. S.; Tagmount, A.; Hejazi, N. S.; Hubbard, A. E.; Zhang, L.; Vulpe, C. D. Functional Profiling Identifies Determinants of Arsenic Trioxide Cellular Toxicity. *Toxicol. Sci.* **2019**, *169* (1), 108–121.
- (57) Andrews, S. *FastQC: A quality control tool for high throughput sequence data*; Babraham Bioinformatics, 2010. Available online at: <http://www.bioinformatics.babraham.ac.uk/projects/fastqc>
- (58) Li, H.; Handsaker, B.; Wysoker, A.; Fennell, T.; Ruan, J.; Homer, N.; Marth, G.; Abecasis, G.; Durbin, R.; Genome Project Data Processing, S. The Sequence Alignment/Map format and SAMtools. *Bioinformatics* **2009**, *25* (16), 2078–9.
- (59) R Core Team. *R: A language and environment for statistical computing*; R Foundation for Statistical Computing: Vienna, Austria, 2020.
- (60) McCarthy, D. J.; Chen, Y.; Smyth, G. K. Differential expression analysis of multifactor RNA-Seq experiments with respect to biological variation. *Nucleic Acids Res.* **2012**, *40* (10), 4288–97.
- (61) Robinson, M. D.; McCarthy, D. J.; Smyth, G. K. edgeR: a Bioconductor package for differential expression analysis of digital gene expression data. *Bioinformatics* **2010**, *26* (1), 139–40.
- (62) Love, M. I.; Huber, W.; Anders, S. Moderated estimation of fold change and dispersion for RNA-seq data with DESeq2. *Genome Biol.* **2014**, *15* (12), 550.
- (63) Benjamini, Y.; Hochberg, Y. Controlling the False Discovery Rate: A Practical and Powerful Approach to Multiple Testing. *Journal of the Royal Statistical Society. Series B (Methodological)* **1995**, *57* (1), 289–300.
- (64) Doench, J. G.; Fusi, N.; Sullender, M.; Hegde, M.; Vaimberg, E. W.; Donovan, K. F.; Smith, I.; Tothova, Z.; Wilen, C.; Orchard, R.; Virgin, H. W.; Listgarten, J.; Root, D. E. Optimized sgRNA design to maximize activity and minimize off-target effects of CRISPR-Cas9. *Nat. Biotechnol.* **2016**, *34* (2), 184–191.
- (65) Jung, J.; Konermann, S.; Gootenberg, J. S.; Abudayyeh, O. O.; Platt, R. J.; Brigham, M. D.; Sanjana, N. E.; Zhang, F. Genome-scale CRISPR-Cas9 knockout and transcriptional activation screening. *Nat. Protoc.* **2017**, *12* (4), 828–863.